Optimal Combustion to Counteract Ring Formation in Rotary Kilns

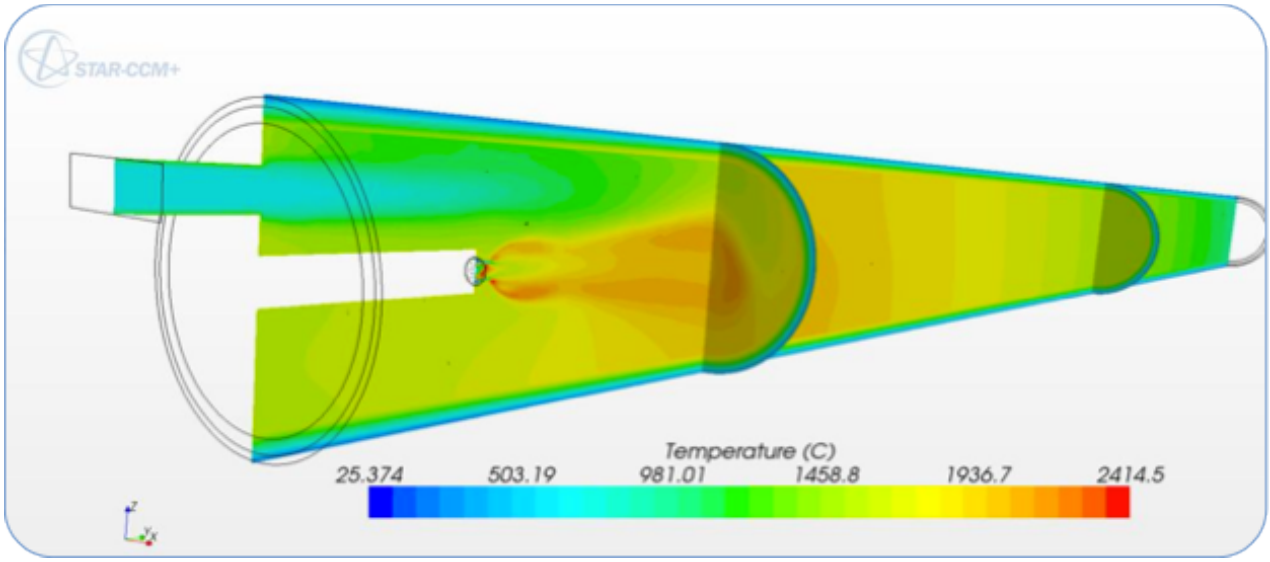

Michele Pisaroni
michele.pisaroni@gmail.com

Scientific Computing Group, Delft Institute of Applied Mathematics,
Faculty of Electrical Engineering, Mathematics and Computer Science
Delft University of Technology, The Netherlands

Abstract

Avoiding the formation of rings in rotary kilns is an issue of primary concern to the cement production industry. We developed a numerical combustion model that revealed that in our case study rings are typically formed in zones of maximal radiative heat transfer. This local overheating causes the overproduction of the liquid phase of the granular material that tends to stick to the oven's wall and to form rings. To counteract for this phenomenon, we propose to increase the amount of secondary air injected to cool the oven. Experimental validation at the plant has repeatedly shown that our solution is indeed effective. For the first time in years, the kiln has been operation without unscheduled shutdowns, resulting in a monthly five-digits cost saving.

Keywords: rotary kiln, combustion model, ring formation.

I. INTRODUCTION

A. Rotary kilns

A rotary kiln is a long horizontal cylinder slightly inclined tilted on its axis. The objective of a rotary kiln is to drive the specific bed reactions, which, for both kinetic and thermodynamic reasons, require high bed temperature. In direct-fired kilns, the energy necessary to raise the bed temperature to the level required for the intended reactions originates with the combustion of hydrocarbon fuels in the freeboard near the heat source of burner. This energy is subsequently transferred by heat exchange between the gas phase and the bed. The material to be processed is fed into the upper end of the cylinder. As the kiln rotates, material gradually moves down towards the lower end, and may undergo a certain amount of stirring and mixing. Heat transfer between the freeboard and the bed is rather complex and occur by all the paths established by the geometric view factors in radiation exchange. All these manifest themselves into a combined transport phenomenon with the various transport processes coming into play in one application. [2]

In our kiln in Rotterdam we produce Calcium Aluminate Cement (CAC), a very white, high purity hydraulic bonding agents providing controlled setting times and strength development for today's high performance refractory products.

The cement is made by fusing together a mixture of a calcium bearing material (limestone) and an aluminium-bearing material. The calcined material drops into the "cool end" of the kiln. The melt overflows the hot end of the furnace into a cooler in which it cools and solidifies (Fig.1). The cooled material is then crushed and grounded.

One of the primary issues in our production is the ring formation.

B. Ring Formation

As material slides and tumbles through a kiln, a thin layer of dust invariably forms on the surface of the refractory lining. Some zones of the kiln may be particularly prone to particle accumulation and the combined effect of particular thermal and flow conditions results in the formation of cylindrical deposits, or *rings*. As the ring grows thicker, the available opening of the kiln is decreased, hindering the flow of lime product and flue gasses through the kiln.

In our CAC (Calcium Aluminate Cement) kiln in Rotterdam we observed in particular *front-end / mid-kiln rings* [9]. They are located close to the burner and are presumably caused by the high temperature in this area, particularly when the refractory surface is overheated by direct impingement of the burner flame. These are the most common and also the most troublesome type of rings. They cannot be reached from outside the kiln and is therefore impossible to remove while the kiln is in operation.

In severe cases, rings grow rapidly and cause unscheduled shutdowns of the kiln. Depending on the severity of the problem, maintenance labour, make-up lime purchase, and lime mud disposal can bring the cost of a ring outage to 150,000 € per shout down. In the last 3 years an average of 1 ring formation per month was registered, 70% of which caused shut down of the kiln.

II. COUNTERACTING RING FORMATION

Even though the temperature inside the kiln is obviously an important factor in ring formation, it cannot be measured easily. Since the gas temperature profile along the kiln varies significantly with burner configurations, fuel, moisture content and the insulating lining it is difficult to obtain the exact temperature at which rings are formed.

To solve this problem we started our analysis from the material phase diagram [3] (Fig. 2). Rings are

caused by too much liquid phase in the region of the kiln where we expect the maximum temperature and radiative heat transfer on the interface between the gas and insulating lining. We decided to run our simulation with an empty kiln and analyse the temperature of the gas-lining interface as a parameter to understand the amount of liquid phase in the kiln. This simplification allow to reduce the complexity of the model and in particular can give us a valid estimation of the amount of heat produced by the flame and exchanged with the granular material flowing in the kiln.

We decided to recreate the thermal and fluid conditions in an empty kiln model to reduce the computational efforts needed to simulate the granular moving bed, that occupies no more than 5% of the volume of the kiln.

III. COMPUTATIONAL MODEL

In the kiln we examine a flame projected from a burner-pipe inside the kiln generates the hot gases (Fig.3). In the hot zone of the kiln we inject hot air from an air inlet placed on the top of the burner, natural gas from the injectors of the burner and a small amount of cold air form the cooling slot placed around the inlets to cool down the surface of the burner. Assuming that it is not possible to modify radically the geometry of the kiln, we were interested in finding out if it was possible to achieve an effective reduction of ring formations, a setup of the kiln able to counteract the growing of rings and keep the temperature and the conditions as much as possible close to the optimum for the production. Hence we decide to investigate in the effects of the secondary air injection effects on the flame and lining temperature.

We decided to run the simulation on a full 3D geometry of the kiln because the flow conditions inside the kiln are not symmetric as a result of the presence of the rectangular air intake.

The geometry of the complete kiln is shown in Fig. 4 and Fig.5.

A. Grid Generation

We used a polyhedral mesh with refinement in the critical zone (Fig.6, Fig.7 and Fig.8). At the end of the refinement we have 2.8 million of cells.

Polyhedral mesh provide a balanced solution for complex mesh generation problems. They offer the same automatic meshing benefits as tetrahedral while overcoming some disadvantages. A major advantage of polyhedral cells is that they have many neighbours (typically of order 10); gradients can be much better approximated than with tetrahedral cells. More neighbours obviously means more storage and computing operations per cell, but this is more than compensated by a higher accuracy. Polyhedral cells are also less sensitive to stretching than tetrahedra. For a polyhedron with 12 faces, there are six optimal directions, which, together with the larger number of neighbours, leads to a more accurate solution with a lower cell count. A more detailed analysis of polyhedral mesh can be found in Peric (2004) [5].

B. Governing Equations

Turbulent combustion arises from the two-way interaction between chemistry and turbulence. When a flame interacts with a turbulent flow, turbulence is modified by combustion because of the strong flow accelerations through the flame front induced by heat release, and because of the large changes in kinematic viscosity associated with temperature changes.

Compared to premixed flames, turbulent non-premixed flames exhibit some specific features that have to be taken into account. Non-premixed flames do not propagate: they are located where fuel and oxidizer meet. This property has consequences on the chemistry/turbulence interaction: without propagation speed, a non-premixed flame is unable to impose its own dynamics on the flow field and is more sensitive to turbulence. Molecular diffusion may also be strongly affected (differential diffusivity

effects).

We use the following list of models in our computations: C.1 Turbulence Model: Realizable K-epsilon, C.2 Chemical Reaction Model, C.3 Combustion Model: Eddy Break Up (EBU), C.4 Radiation Model: Participating Media (DOF). These models are described in detail in Appendix 2.

IV. COMPUTATIONAL RESULTS

In this section we present the computational results obtained with the models described in the previous section. The computation was done with STAR-CCM+ [1]. We run this model on a 10-node cluster for 3500-4000 iterations. The time needed for a single computation was 3-3.5 days.

We present here 2 configuration of the kiln: STD_Config is the standard configuration used in the past years in our plant with a volume air-fuel ratio of 9 and H_Air is the new configuration with a volume air-fuel ratio of 12.

Scenario	INLET_AIR	FUEL	AIR/FUEL RATIO (A/F)
STD_Config	4230 [m^3/h]	470 [m^3/h]	9
H_Air	5655 [m^3/h]	470 [m^3/h]	12

A. Standard Configuration (STD_Config)

With standard configuration we mean that we run our model with all the parameters set as in the standard production situation.

The first key result is the temperature profile in the kiln shown in Fig.10. In the analysis of ring

formation one of the most interesting parameter that must be taken into account is the temperature at the interface between the hot gas and the solid wall (Fig.11). It is well shown that the hottest zone is placed in a particular position exactly in the interval at 4.5-7 m from the burner. This is also the interval where in reality we can find the most severe ring formations in our kiln. In Fig. 11 it is possible to see that the flame (represented as the iso-surface with concentration of CH4 higher than 0.01) peak temperature is placed exactly near the zone where we measure the maximum wall temperature.

The second key result is the incident radiation on the same hot gas-solid interface. A particular zone (Fig.12 and Fig.13) is exactly placed in the highest temperature zone. The material that is flowing in this section absorbs the maximum heat due to this peak of radiation produced by the flame propagating above it. It is reasonable to hypnotize that the liquid phase of material in this zone is so high that the material becomes sticky and attack the solid wall.

B. Higher Air-Fuel Ratio (H_Air)

With higher air-fuel configuration we mean that we run our model with the volume air-fuel ratio set to 12. We keep the injectors of fuel and the cooling air of the burner set as in the standard configuration.

We observe that in this configuration the gas temperature is lower than in the standard case (Fig. 14). The blue zone on the top, due to the secondary air injection, propagates further because more air is injected in the kiln. The secondary air injection acts as a cooler for the wall. Also the incident radiation in the gas-solid interface is lower and the region with maximum radiation is smaller compared with the previous case (Fig.16 and Fig.17).

The material that is flowing in this section absorbs less heat due to this lower radiation. It is reasonable to hypnotize that the liquid phase of material in this zone is lower and that the material cannot attack the wall.

In an X-Y plot we can easily see the temperature and the radiation peak in the gas-solid interface are lower then the previous case (c.a -5% Temperature and -11% Incident Radiation) (Fig.18 and Fig.19).

V. EXPERIMENTAL VALIDATION AT PLANT

The reported simulation model, shows that the flame peak temperatures and the interface between gas and solid can be reduced significantly. The hypothesis is that reducing the flame temperature will result in reduction of heat-transfer via radiation, the clinker bed is below it's melting regime. That will stop the growing of the ring dam.

On August the 28th 2011, a severe ring formation was reported from the plant (Fig.20). After assessing the situation, it was decided to increase the A/F ratio substantially (from 9 to 12). The effects of A/F ratio 12 that we were expecting due to previous numerical calculation:

- flame temperature peaks down
- interface hot gas-solid wall reduced
- no significant change in flow pattern
- radiative heat transfer reduced
- melting and growing of ring stopped

We observed that:

- 4 hours later it can be seen that ring stops growing (Fig. 21)
- 24 hours later the ring size stabilized and started to decrease due to breaking of lumps (Fig.22)
- 40 hours later the kiln remain stable in operation (Fig. 23)

Several days later, the kiln ring diminishes slowly until it was almost destroyed. When the growing of

the ring is stopped and we reach a temperature at which the liquid phase is very low the vibration due to the drive gears of the kiln and the rotation gradually breaks lumps from the ring and after 40 hours the ring is almost destroyed.

ACKNOWLEDGEMENT

We thank Marco Talice for his advice worth more than platina and the CD-ADAPCO London office for the support in using their software.

VI. CONCLUSION

We developed a numerical model allowing to access the effectiveness of measures implemented to counteract the formation of rings in a rotary cement kiln used in use by Almatis B.V. in Rotterdam. In this three-dimensional combustion model, the gas flow, the temperature profile, radiative heat distribution and the concentration of hydro-carbon species in the kiln is taken into account. Simulations show that increasing the volume air-fuel ratio reduces peaks in radiative heat transfer in zones critical to ring formation. This reduction results in turn in less heat being absorbed by the granular material bed, effectively reducing the amount of material liquid phase prone to sticking to the kiln's surface and to forming rings. The validity of our model has been experimental observed at the Almatis plant in Rotterdam. Since August 28th, 2010, the kiln has been operation without unscheduled shut-downs, resulting in a monthly five-digits cost saving.

Appendix 1

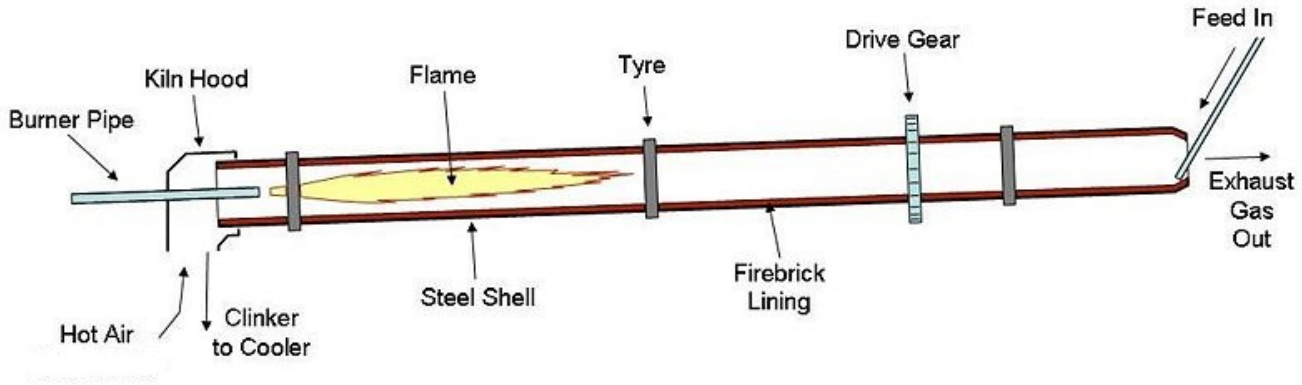

Fig.1. General layout of a direct fired, countercurrent feed rotary kiln.

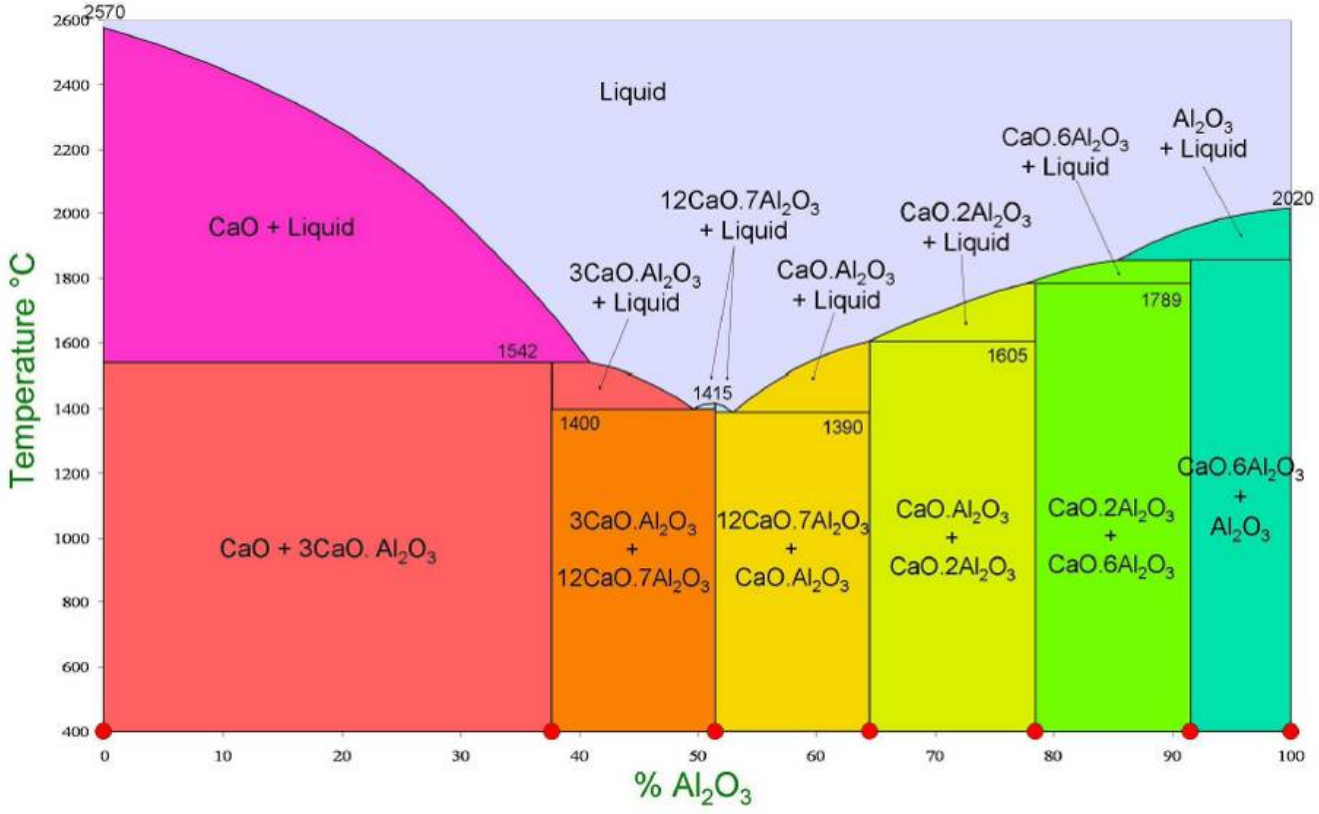

Fig.2. Phase diagram

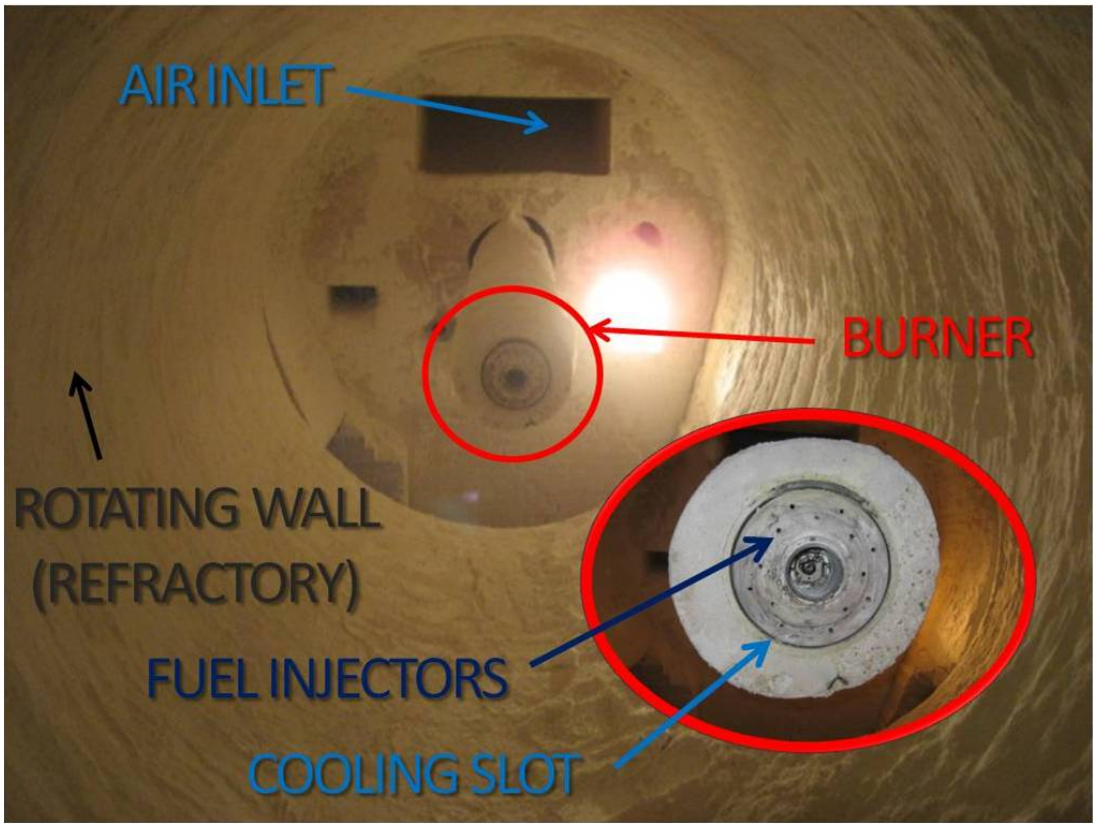

Fig.3. Burner setup

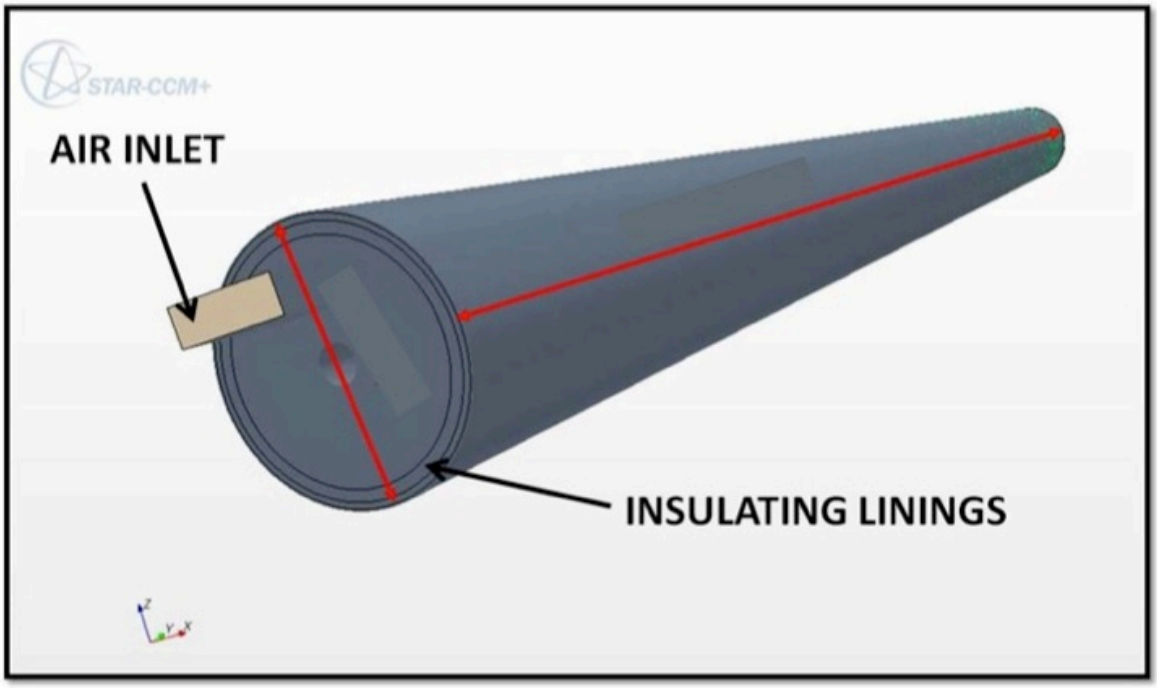

Fig.4. Outside view of the kiln

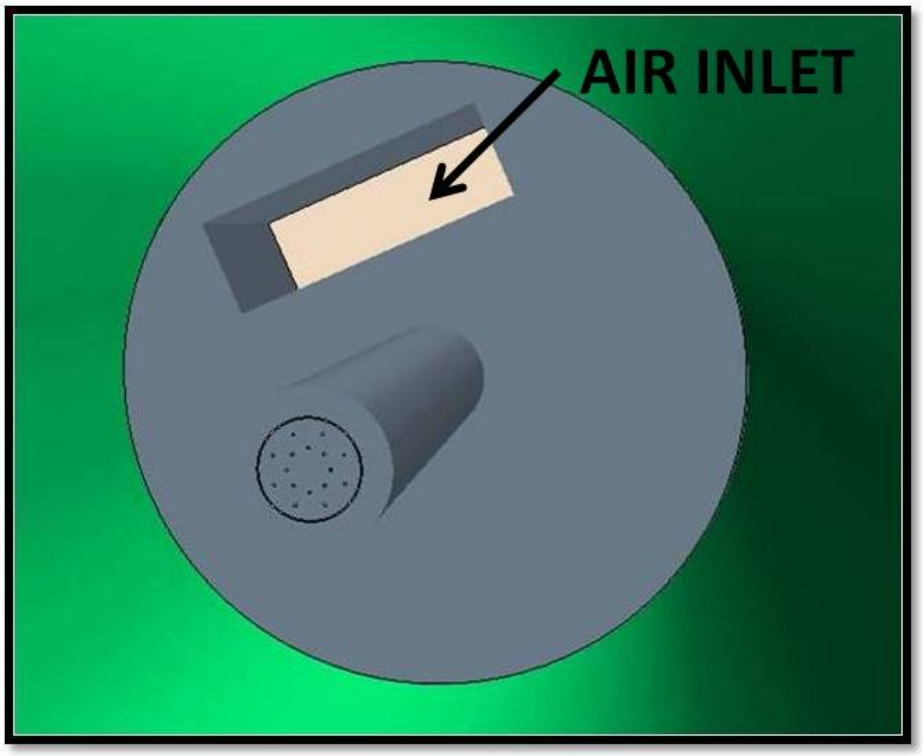

Fig.5. Burner zone

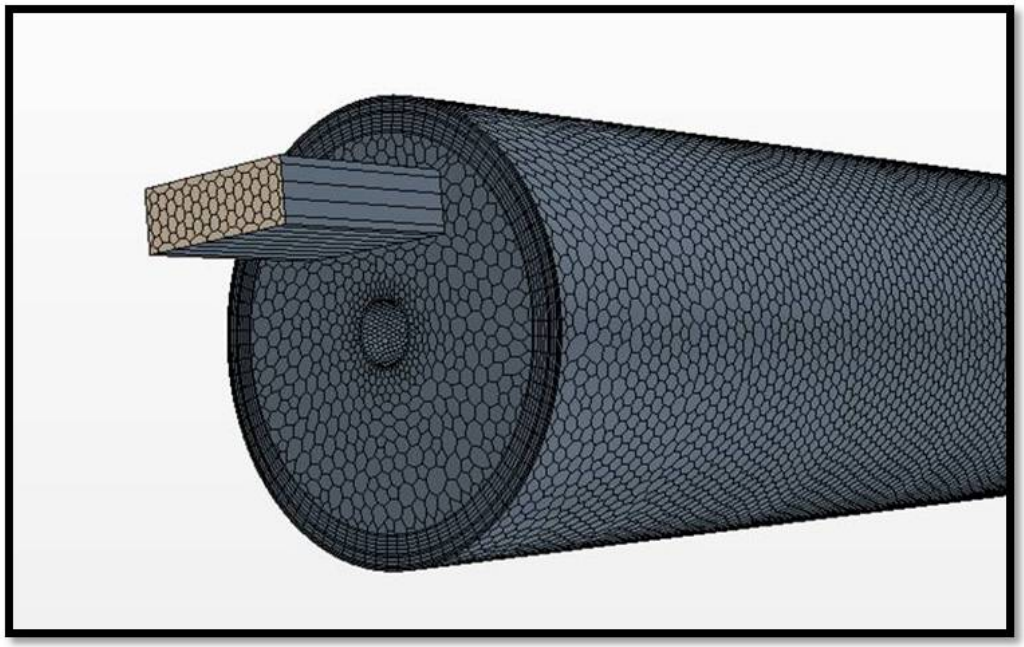

Fig.6. Outside view of the grid

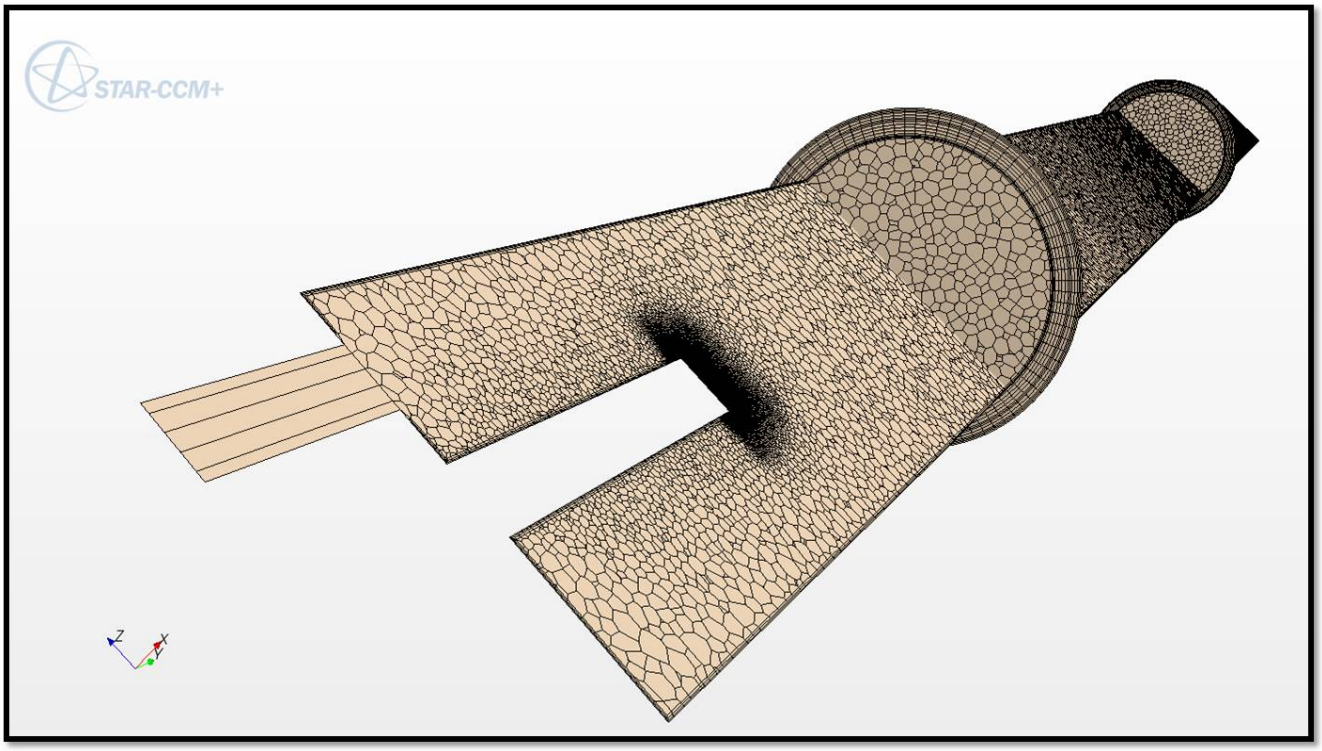

Fig.7. Interior refinment

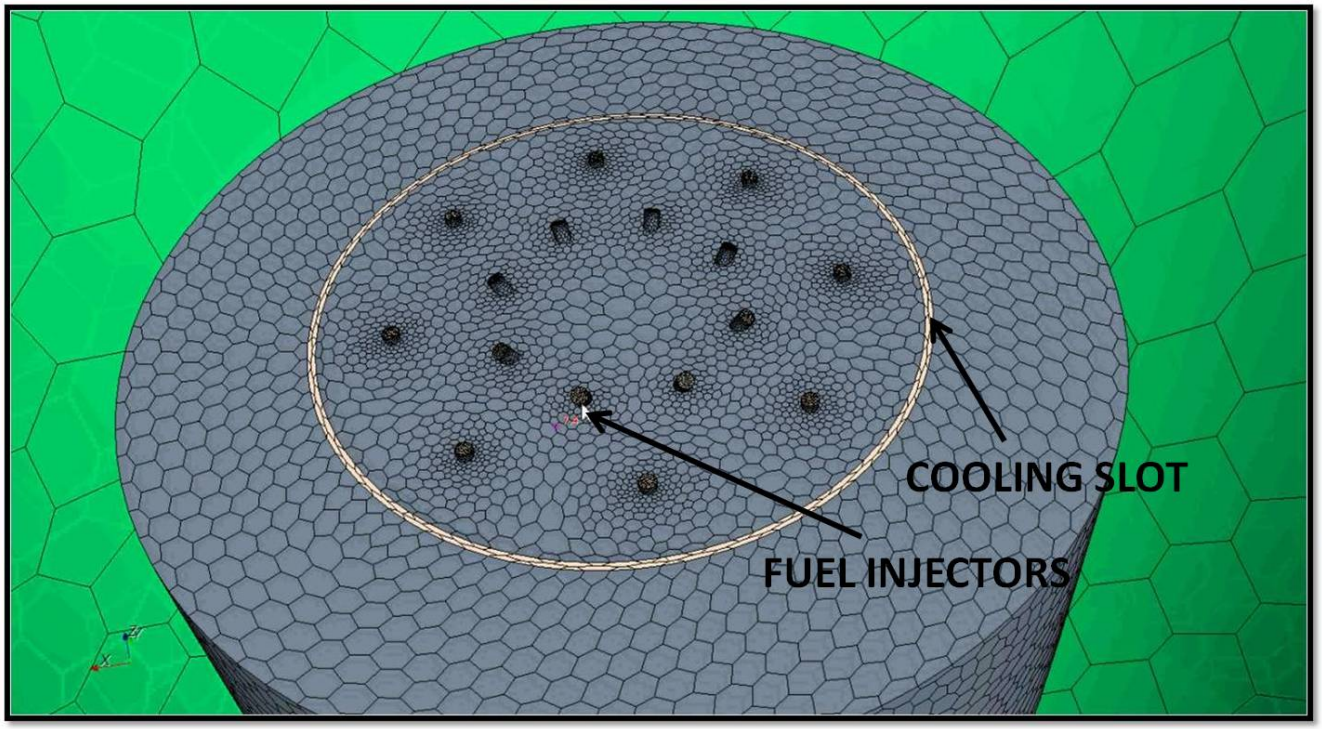

Fig.8. Details of the grid in the burner zone

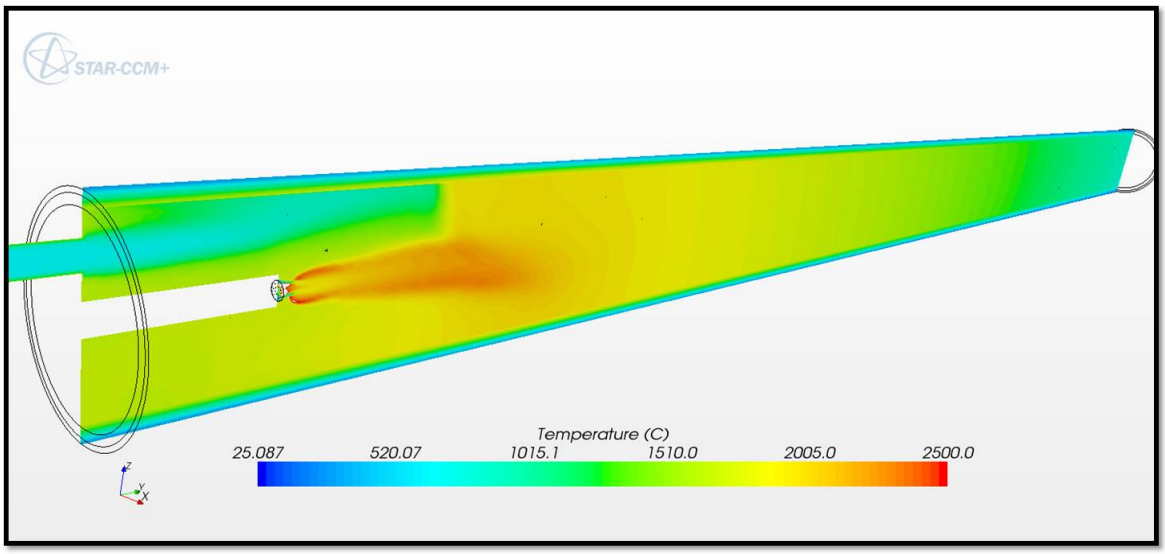

Fig.10. Temperature profile in the axial section (A/F=9)

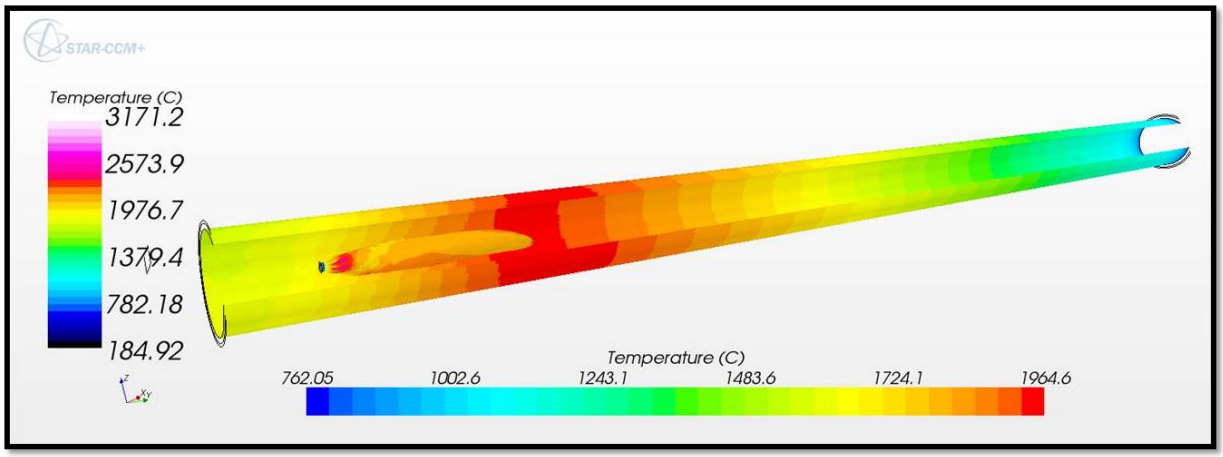

Fig.11. Temperature of Hot Gas – Solid Wall interface (A/F=9)

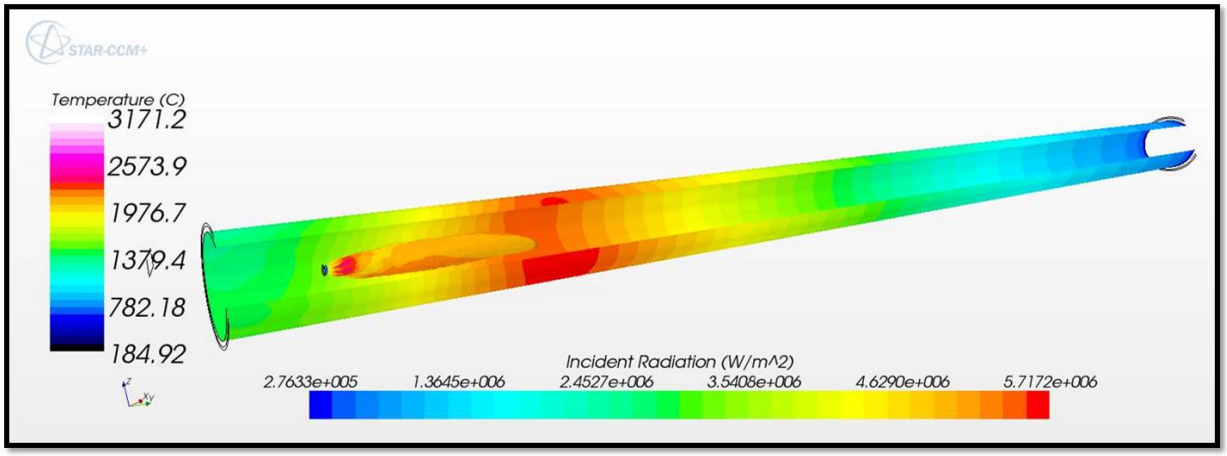

Fig.12. Incident radiation Hot Gas – Solid Wall interface (A/F=9)

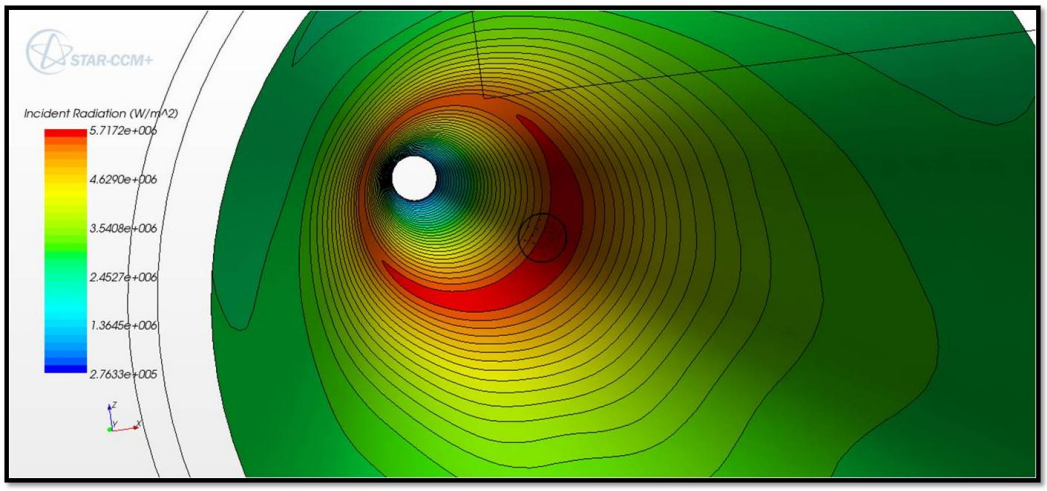

Fig.13. Incident radiation Hot Gas – Solid Wall interface (A/F=9)

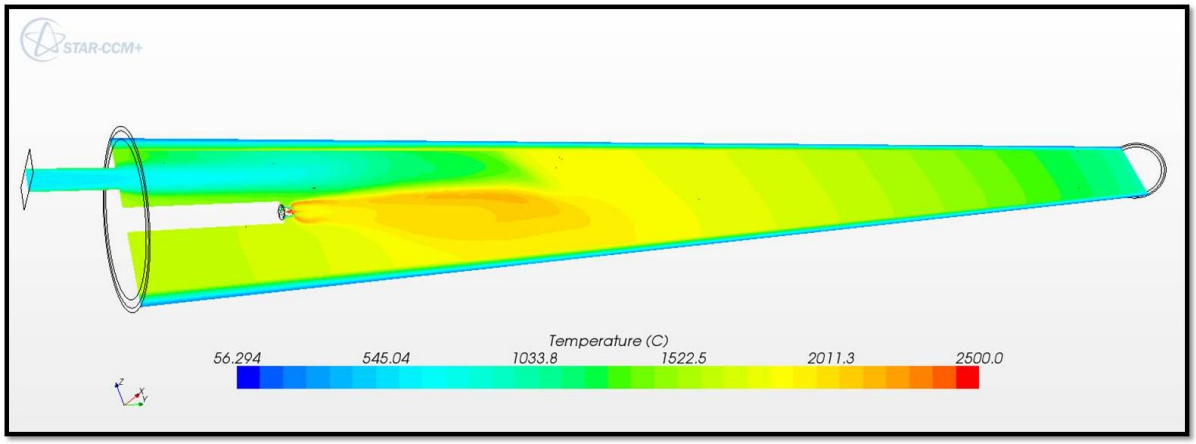

Fig.14. Temperature profile in the axial section (A/F=12)

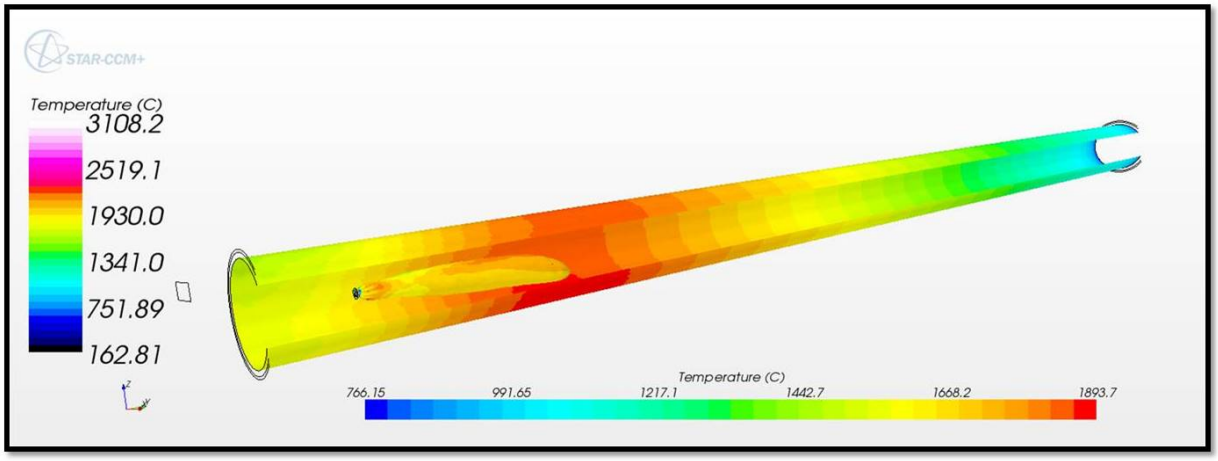

Fig.15. Temperature of Hot Gas – Solid Wall interface (A/F=12)

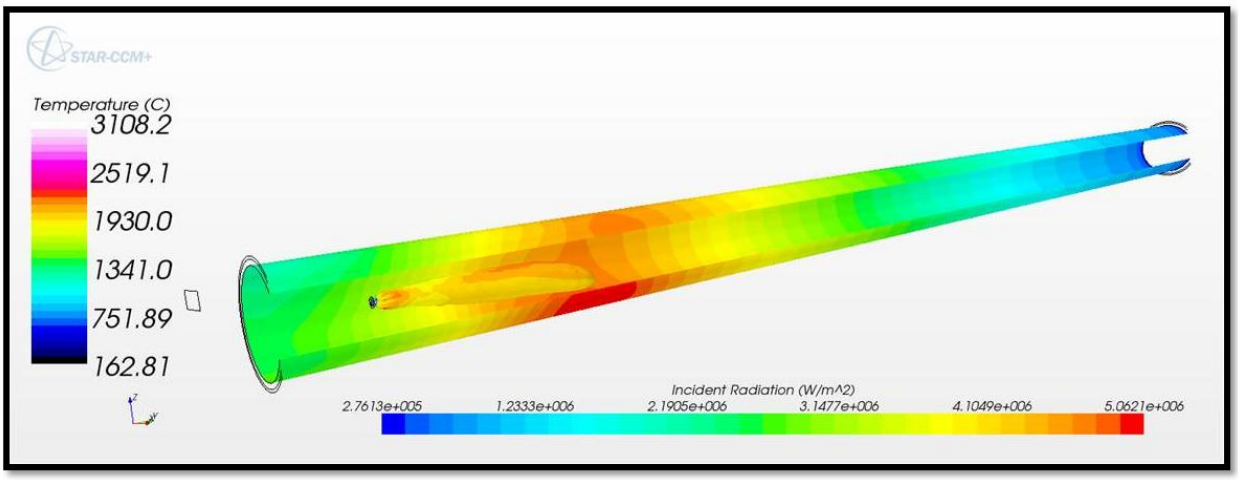

Fig.16. Incident radiation Hot Gas – Solid Wall interface (A/F=12)

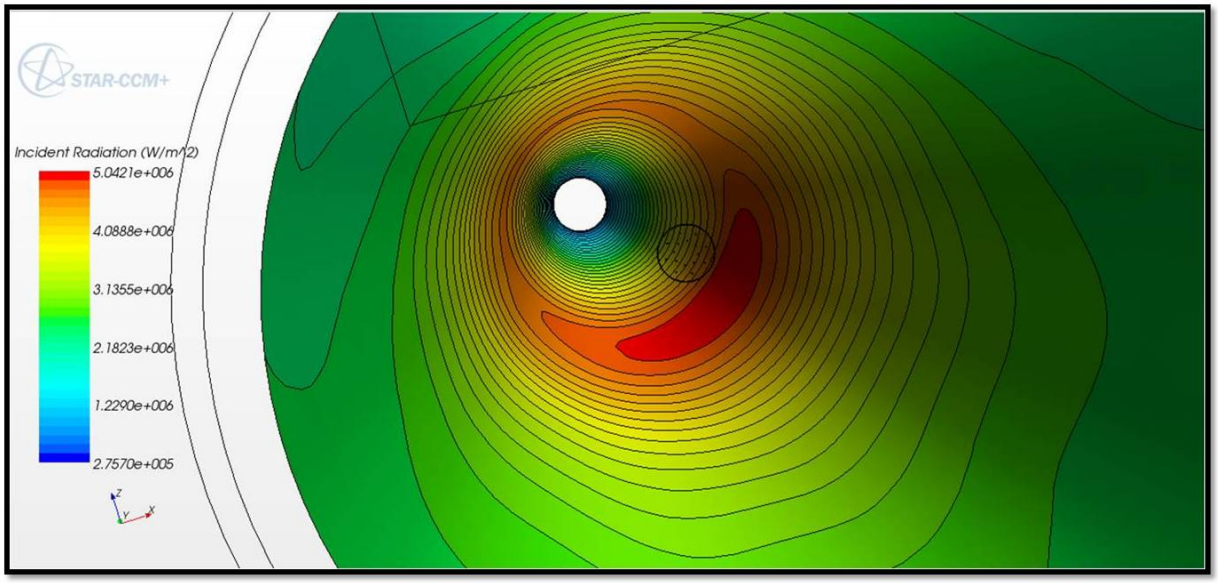

Fig.17. Incident radiation Hot Gas – Solid Wall interface (A/F=12)

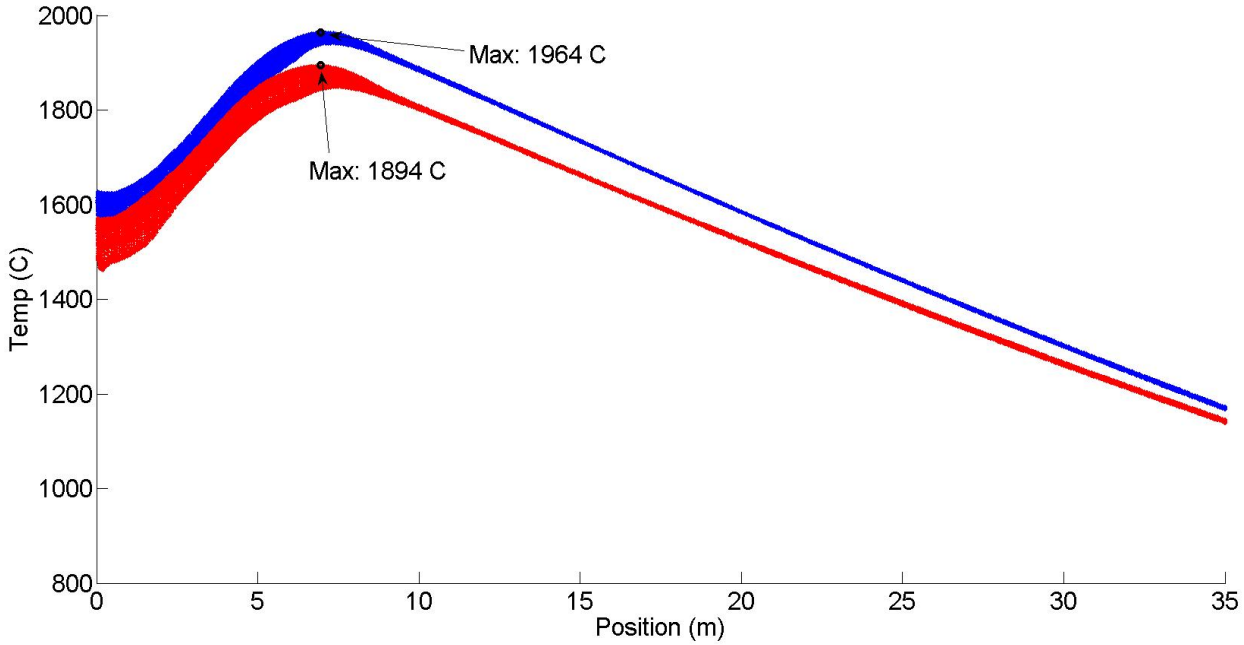

Fig.18. Temperature vs position (blue A/F=9, red A/F=12)

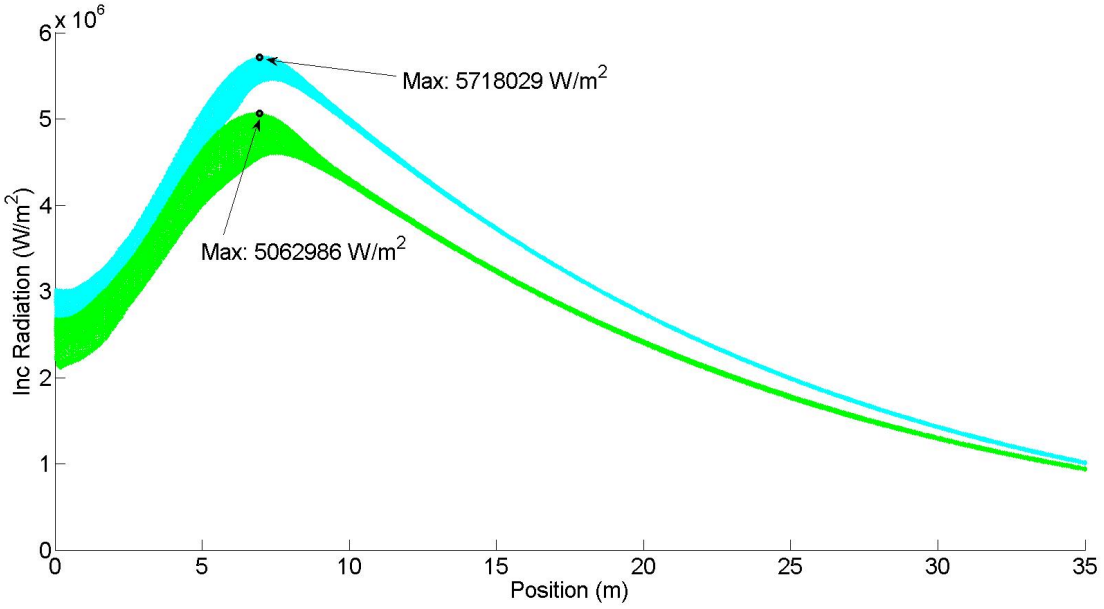

Fig.19. Incident radiation vs position (cyan A/F=9,greenA/F=12)

Fig.20. Ring structure at A/F=9

Fig.21. Ring structure after 4 hours the imposition of A/F=12

Fig.22. Ring structure after 24 hours the imposition of A/F=12

Fig.23. Kiln returned in a stable condition after 40 hours

Appendix 2

C.1 Turbulence Model

The description of the turbulent flows in non-premixed combustion processes using Computational Fluid Dynamics (CFD) may be achieved using three levels of computations: Reynolds Averaged Navier Stokes (RANS), Large Eddy Simulations (LES) or Direct Numerical Simulations (DNS). In current engineering practice, RANS is extensively used because it is less demanding in terms of resources but the closure models describing turbulence and combustion limit its validity. The advantage of RANS is its applicability to any configuration and operating conditions. Considering the complexities and the dimensions of our kiln, the only feasible choice was RANS.

To obtain the Reynolds-Averaged Navier-Stokes (RANS) equations, the Navier-Stokes equations for the instantaneous velocity and pressure fields are decomposed into a mean value and a fluctuating component [6].

A K-Epsilon turbulence model is a two-equation model in which transport equations are solved for the turbulent kinetic energy k and its dissipation rate ε. Various forms of the K-Epsilon model have been in use for several decades, and it has become the most widely used model for industrial applications. In our case we used a **Realizable K-Epsilon model**. A critical coefficient of the model is expressed as a function of mean flow and turbulence properties, rather than assumed to be constant as in the standard model. This allows the model to satisfy certain mathematical constraints on the normal stresses consistent with the physics of turbulence (realizability).

The two equations for the model are:

$$\frac{\partial}{\partial t}(\rho k) + \frac{\partial}{\partial x_i}(\rho k u_i) = \frac{\partial}{\partial x_j}\left[\left(\mu + \frac{\mu_t}{\sigma_k}\right)\frac{\partial k}{\partial x_j}\right] + P_k + P_b - \rho\varepsilon - Y_M + S_k \quad (1)$$

for turbulent kilnetic energy k

$$\frac{\partial}{\partial t}(\rho\varepsilon) + \frac{\partial}{\partial x_i}(\rho\varepsilon u_i) = \frac{\partial}{\partial x_j}\left[\left(\mu + \frac{\mu_t}{\sigma_\varepsilon}\right)\frac{\partial \varepsilon}{\partial x_j}\right] + C_{1\varepsilon}\frac{\varepsilon}{k}(P_k + C_{3\varepsilon}P_b) - C_{2\varepsilon}\rho\frac{\varepsilon^2}{k} + S_\varepsilon \quad (2)$$

for dissipation ε.

C.2 Chemical Reactions Model

The flame projected from the burner-pipe inside the kiln is continuously fed by the injection of natural gas (more than 90 % of methane (CH4)) that reacts with hot (500-600 C) air (23% of O2) injected from the top window visible in Fig.3.

Consider a chemical system of N species reacting through M reactions:

$$\sum_{k=1}^{N} v'_{kj}\mathcal{M}_k \iff \sum_{k=1}^{N} v''_{kj}\mathcal{M}_k \qquad for \quad j = 1, M \quad (3)$$

where M_k is a symbol for species k, v'_{kj} and v''_{kj} are molecular stoichiometric coefficients of species k

in reaction j. Consider mass reaction rates, for species k, $\dot{\omega}_k$ is the sum of rates $\dot{\omega}_{kj}$ produced by all M reactions:

$$\dot{\omega}_k = \sum_{j=1}^{M} \dot{\omega}_{kj} = W_k \sum_{j=1}^{M} v'_{kj} Q_j \qquad with \qquad Q_j = \frac{\dot{\omega}_{kj}}{W_k v_{kj}} \quad (4)$$

where Q_j is the rate of progress of reaction j. The progress rate Q_j of reaction j is written:

$$Q_j = K_{fj} \prod_{k=1}^{N} \left(\frac{\rho Y_k}{W_k} \right)^{v'_{kj}} - K_{rj} \prod_{k=1}^{N} \left(\frac{\rho Y_k}{W_k} \right)^{v''_{kj}} \quad (5)$$

where K_{fj} and K_{rj} are the forward and reverse rates of reaction j.

These rate constants are the central problem of combustion modeling. They are usually modeled using the empirical Arrhenius law:

$$K_{fj} = A_{fj} T^{\beta_j} exp\left(-\frac{E_j}{RT} \right) = A_{fj} T^{\beta_j} exp\left(-\frac{T_{aj}}{T} \right) \quad (6)$$

Expressing the individual progress rates Q_j for each reaction means providing data for the pre-exponential constant A_{fj}, the temperature exponent β_j and the activation temperature T_{aj} (or the activation energy EJ = RT_{aj}). In numerical approach for reacting flows, the chemical scheme (or mechanism) is one database of data, which must be available for the computation. In our calculations we used and tested different reaction mechanisms; some are very simple and contains only the

reactions of methane and few species, other more detailed mechanisms contain also other alkanes reactions and more species. Since it is well known that EBU degrades its global accuracy as the number of species increases, we decided to restrict our calculations to a 5-step mechanism with 14 species.

C.3 Combustion Model

We have now to link the reactions and their proprieties with the turbulent flow produced by the flame and vice versa. To do so a combustion model is needed. The purpose of combustion models is to calculate the reaction state space and the quantities they influence: density, viscosity, and temperature. A large chemical reaction set can span a wide range of time and length scales. Resolving all the length and time scales affecting the grid-mean properties in a reacting flow system demands computational resources beyond those currently available. We therefore need combustion models to account for the processes that occur at length and time scales below what we can resolve on a numerical simulation grid.

The choice of combustion model is decided by knowing the Damkohler number. When the Damkohler number is very large, as in the case of the kiln, the turbulent mixing that brings reactants together at the molecular scale controls the reaction rate. In this limit, the **Standard Eddy Break Up (EBU)** model is fairly accurate because it assumes that the reaction occurs instantaneously upon micromixing.

EBU combustion model track individual mean species concentrations on the grid through transport equations. The reac- tion rates used in these equations are calculated as functions of the mean species concentrations, turbulence characteristics and, depending on the specific model used, temperature. A mean enthalpy equation is solved in addition to the species transport equations. The mean temperature, density and viscosity are then calculated knowing the mean enthalpy and species concentra- tions. In the standard EBU, individual species in the global reaction are assumed to be transported at different

rates according to their own governing equations. These are derived from the instantaneous governing equations for species i.

$$\frac{\partial}{\partial t}(\rho\chi Y_i) + \nabla \cdot (\rho U Y_i - F_i) = S_i \tag{7}$$

in which Fi is the diffusion flux, Di is the molecular diffusivity of species i, and S_i is the reaction rate. The standard EBU model uses the time-average of the instantaneous governing equations:

$$\frac{\partial}{\partial t}(\rho\chi \overline{Y}_i) + \nabla \cdot (\rho U \overline{Y}_i - \overline{F}_i) = \overline{S}_i \tag{8}$$

where F_i now includes the effect of turbulent diffusion and is defined as:

$$\overline{F}_i = \left(D_i + \frac{\mu_t}{Sc_i} \right) \nabla \overline{Y}_i \tag{9}$$

where μ_t is the turbulent diffusivity and Sc_i is the turbulent Schmidt number. The reaction rate is modeled through an expression that takes the turbulent micromixing process into account. This is done through dimensional arguments. Thus, for a reaction of the form:

$$v_F F + v_O O \longrightarrow v_{P1} P_1 + v_{P2} P_2 + ... + v_{Pj} P_j \tag{10}$$

the rate of fuel depletion is assumed to be:

$$R_F = -\frac{\rho}{M_F}\left(\frac{1}{\tau_R}\right) A_{ebu}\, min\left\{\overline{Y}_F, \frac{\overline{Y}_O}{s_O}, B_{ebu}\left(\frac{\overline{Y}_{P1}}{s_{P1}} + ... + \frac{\overline{Y}_{Pj}}{s_{Pj}}\right)\right\} \quad (11)$$

The reaction source term for each species can then be obtained from:

$$S_i = M_i \sum_{j=1}^{n_r} v_{ij} R_j \quad (12)$$

C.4 Radiation Model

A **Participating Media Radiation Model (DOF)** is needed to simulate the heat transfer due to radiation. In some cases, thermal radiation can occur only as a surface phenomenon. The media separating the surfaces (such as dry air) is transparent to thermal radiation. However, other as in our kiln we require consideration of participating media. This term refers to media lying between the radiating surfaces that can absorb, emit, and/or scatter thermal radiation.

As radiation travels through a medium, its radiant intensity I in the Ω direction is absorbed and incremented by the intervening material. This process is governed by the radiative transfer equation (RTE) which, written in terms of radiant intensity for a specific wavelength , is given by:

$$\frac{dI_\lambda}{ds} = -\beta_\lambda I_\lambda + k_{a\lambda} I_{b\lambda} + \frac{k_{s\lambda}}{4\pi} \int_{4\pi} I_\lambda(\Omega)\, d(\Omega) + k_{pa\lambda} I_{pb\lambda} + \frac{k_{ps\lambda}}{4\pi} \int_{4\pi} I_\lambda(\Omega)\, d(\Omega) \tag{13}$$

$$I_{b\lambda} = \frac{2C_1}{\lambda^5 \left(e^{C_2/\lambda T} - 1\right)} \tag{14}$$

When the absorption and scattering coefficients of the medium are independent of wavelength, the medium is called grey. In that case, the RTE can be integrated over wavelength to produce a wavelength independent equation. The boundary condition applied to the RTE for diffusely emitting (with emissivity $\varepsilon_{w\lambda}$) and reflecting (with reflectivity $\rho_{w\lambda}$) boundaries is, for each wavelength:

$$I_\lambda(s) = \varepsilon_{w\lambda} I_{w\lambda} + \frac{\rho_{w\lambda}}{\pi} \int_{(m \cdot s' < 0)} I_\lambda(s') \left| n \cdot s' \right| d\Omega \tag{15}$$

The radiant heat flux in a particular direction q_r is given by the integration of the radiant intensity over all solid angles and over the wavelength spectrum:

$$q_r(r) = \int_0^\infty \int_{4\pi} I_\lambda(s) s \;\; d\Omega \, d\lambda \tag{16}$$

The radiation solution is coupled to the fluid dynamic solution through the divergence of the radiative heat flux. This term exchanges energy between the fluid and the radiant energy field. Given the intensity field, the divergence of the heat flux is computed as:

$$\nabla \cdot q_r = \int_0^\infty k_{a\lambda} \left(4\pi I_{b\lambda} - \int_{4\pi} I_\lambda \, d\Omega \right) \, d\lambda \qquad (17)$$

The discrete ordinates method solves field equations for radiation intensity associated with a fixed direction s, represented by a discrete solid angle.

A detailed description of the method can be found in Modest [4] and Siegel and Howell [8]. As a result of Eqn. (20), the form of these ordinate equations (for each wavelength band) is:

$$s_i \cdot \nabla I_{i\Delta\lambda} = -\beta_{\Delta\lambda} I_{i\Delta\lambda} + k_{a\Delta\lambda} I_{b\Delta\lambda} + \frac{k_{s\Delta\lambda}}{4\pi} \sum_{j=1}^{n} w_j I_{j\Delta\lambda} + \overline{k}_{pa\Delta\lambda} I_{pb\Delta\lambda} + \frac{\overline{k}_{ps\Delta\lambda}}{4\pi} \sum_{j=1}^{n} w_j I_{j\Delta\lambda} \qquad (18)$$

In the above equation, $\Delta\lambda$ represents a wavelength band from λ_m to λ_n. The black body emission in this band is given by:

$$I_{b\Delta\lambda} = \int_0^{\lambda_n} I_{b\lambda} \, d\lambda - \int_0^{\lambda_m} I_{b\lambda} \, d\lambda \qquad (19)$$

The equivalent particle absorption and scattering coefficients are given as:

$$\overline{k}_{pa\Delta\lambda} = \sum_i Q_{a,i} N_i \frac{\pi d_i^2}{4}, \quad \overline{k}_{ps\Delta\lambda} = \sum_i Q_{s,i} N_i \frac{\pi d_i^2}{4} \qquad (20)$$

where i indicates the parcel index number. The transport equation for each ordinate direction is discretized and solved independently. The angularly discretized boundary conditions take the form:

$$I_{i\Delta\lambda,w} = \varepsilon_{w\Delta\lambda} I_{b\Delta\lambda} + \frac{\rho_{w\Delta\lambda}}{\pi} \sum_{(n\cdot s'<0)} I_{j\Delta\lambda} \left| n \cdot s'_j \right|_w \qquad (21)$$

The reflection term represents summation over incoming (incident) ordinate directions. The discretized form of this source term at any cell is:

$$-\nabla \cdot q_r = \sum_\lambda k_{a\Delta\lambda} \left(\sum_{j=1}^{n} 4 w_j I_{j\Delta\lambda} - 4\pi I_{b\Delta\lambda} \right) \qquad (22)$$

The net absorption rate of radiative energy by all particles within a given cell is given by:

$$-\nabla \cdot q_{pr} = \sum_\lambda \overline{k}_{a\Delta\lambda} \left(\sum_{j=1}^{n} 4 w_j I_{j\Delta\lambda} - 4\pi I_{pb\Delta\lambda} \right) \qquad (23)$$

REFERENCES

[1] *Star-CCM+Vers6.06.011UserGuide,2011.*

[2] Akwasi A Boateng. *Rotary Kilns: Transport Phenomena and Transport Processes.* Butterworth-Heinemann, 1st edition, 2006.

[3] Taylor H.F.W. *Cement Chemistry.* Academic Press, 1990.

[4] M.F.Modest.RadiativeHeatTransfer.McGraw-Hill,NY,1993.

[5] M. Peric. Flow simulation using control volumes of arbitrary polyhedral shape. *ERCOFTAC Bulletin, No. 62,* September 2004.

[6] Veynante D. Poinsot, T. *Theoretical and Numerical Combustion.* R.T. Ed- wards, Inc., 2nd edition, 2005.

[7] W. Rodi. Experience with two-layer models combining the k-e model with a one-equation model near the wall. *29th Aerospace Sciences Meeting, January 7-10, Reno, NV, AIAA 91-0216,* 1991.

[8] R. Siegel and J.R. Howell. *Thermal Radiation Heat Transfer.* Hemisphere Publishing Co., Washington, 3rd edition, 1992.

[9] Barham D. Tran H.N. An overview of ring formation in lime kilns. *Tappi Journal,* (74 [1]), 1991.